



ARTICLE

Wavelet Multi-Resolution Interpolation Galerkin Method for Linear Singularly Perturbed Boundary Value Problems

Jiaqun Wang^{1,2}, Guanxu Pan², Youhe Zhou² and Xiaojing Liu^{2,*}

¹School of Management Science and Engineering, Anhui University of Finance and Economics, Bengbu, 233030, China

²Key Laboratory of Mechanics on Disaster and Environment in Western China, The Ministry of Education, College of Civil Engineering and Mechanics, Lanzhou University, Lanzhou, 730000, China

*Corresponding Author: Xiaojing Liu. Email: liuxiaojing@lzu.edu.cn

Received: 14 April 2023 Accepted: 18 September 2023 Published: 30 December 2023

ABSTRACT

In this study, a wavelet multi-resolution interpolation Galerkin method (WMIGM) is proposed to solve linear singularly perturbed boundary value problems. Unlike conventional wavelet schemes, the proposed algorithm can be readily extended to special node generation techniques, such as the Shishkin node. Such a wavelet method allows a high degree of local refinement of the nodal distribution to efficiently capture localized steep gradients. All the shape functions possess the Kronecker delta property, making the imposition of boundary conditions as easy as that in the finite element method. Four numerical examples are studied to demonstrate the validity and accuracy of the proposed wavelet method. The results show that the use of modified Shishkin nodes can significantly reduce numerical oscillation near the boundary layer. Compared with many other methods, the proposed method possesses satisfactory accuracy and efficiency. The theoretical and numerical results demonstrate that the order of the ε -uniform convergence of this wavelet method can reach 5.

KEYWORDS

Wavelet multi-resolution interpolation Galerkin; singularly perturbed boundary value problems; mesh-free method; Shishkin node; boundary layer

1 Introduction

The singularly perturbed boundary value problem originates from fluid mechanics and arises in the mathematical modeling of physical engineering problems. In this study, we consider the following second-order singularly perturbed two-point boundary value problem:

$$\begin{aligned} \varepsilon u''(x) + pu'(x) + qu(x) &= f(x), \quad x \in [a, b] \\ u(a) &= u_a, u(b) = u_b \end{aligned} \quad (1)$$

where ε is a small perturbation parameter that satisfies $0 < \varepsilon \ll 1$, and q is a negative number. A key feature of this problem is the presence of a boundary layer in which the solution undergoes large variations with localized steep gradients as ε approaches zero. We assume that p is a non-zero



parameter, and Eq. (1) features a left-side boundary layer at $x=a$ when $p > 0$, and a right-side boundary layer at $x=b$ for $p < 0$.

The presence of boundary layers makes it challenging to solve singularly perturbed problems using classical numerical methods. Consequently, numerous special schemes have been proposed, including transforming the boundary value problem into an initial value problem [1–3], fitting the finite difference method [4], spline method [5–8], finite element method [9–12], and other methods [13–17]. In recent years, algorithms based on layer-adapted meshes have become powerful tools for solving singular perturbation problems [18–20], such as the Shishkin mesh [7,21–23] and Bakhvalov mesh [24–27].

Over recent decades, meshfree methods that rely only on nodes to make approximations have attracted considerable research interest [28–32]. As pointed out by Li et al. [28], meshfree methods are not only complementary to conventional finite element methods, but they also offer several advantages over mesh-based methods. These advantages include the utilization of higher-order continuous shape functions and the elimination of sensitivity to mesh alignment [31,33,34]. Currently, meshfree methods are widely used for solving singularly perturbed boundary value problems because they can quickly obtain more satisfactory numerical solutions by adding extra approximation nodes in the boundary layer. For example, Shen [35] proposed a local radial basis function (RBF)-based differential quadrature collocation method to solve the singularly perturbed two-point boundary value problem, which avoids highly ill-conditioned dense interpolation matrices. Although that study only discussed uniformly distributed nodes, numerical results showed that the local RBF-based collocation method is more accurate and efficient than the globally supported method. The collocation methods are known for being efficient as no integration is required, but they are less stable and accurate. To reduce errors in the standard element-free Galerkin method near the boundary layer, Zhang et al. [36] proposed the variational multiscale element-free Galerkin method to obtain the numerical solutions of convection-diffusion-reaction equations. Numerical results showed that their method is considerably more accurate than the standard element-free Galerkin method, although slight spurious oscillations persisted near the boundary layer. Zhang et al. [37] later presented a novel adaptive algorithm based on the variational multiscale element-free Galerkin method to overcome this drawback. Although many credible results have been obtained using the aforementioned meshfree methods, they still possess some shortages, such as difficulty in imposing of essential boundary conditions and calculating integrals owing to their shape functions are rational functions and lacking the Kronecker delta property [31].

Wavelet-based methods have gained increasing attention as they are widely and successfully used in practical applications [38–42]. Numerical methods based on wavelets can be divided into three main categories: wavelet finite element [39–40,43], wavelet collocation [44–48], and wavelet Galerkin methods [49–53]. Although wavelet finite element methods have advantages over traditional finite element methods, they still suffer from the same disadvantages in the presence of meshes. Existing wavelet meshfree methods do not require meshes, but they do not guarantee accurate interpolations on non-uniform nodes.

Recently, we proposed a truly meshfree method based on wavelet multiresolution analysis, known as the wavelet multiresolution interpolation Galerkin method (WMIGM) [54,55]. Compared with current meshfree methods, WMIGM possesses several advantages [54,55]:

- (1) The proposed wavelet multiresolution interpolation formula possesses the Kronecker delta function property;
- (2) Polynomial reproduction can be achieved up to $\gamma - 1$ degrees, expressed as linear combinations of shape functions;

- (3) It does not require matrix inversions or ad-hoc parameters;
- (4) The stiffness matrix can be efficiently obtained with an analytical integration method.

A key challenge to solving singularly perturbed boundary value problems is dealing with their singularity, which can lead to numerical instability, oscillations, and spurious solutions [20]. Moreover, the use of uniform nodes in singularly perturbed boundary value problems results in a significant waste of computational effort, as a sufficiently fine mesh is required to accurately capture the rapid variations of the solution near the boundary layer. Therefore, there is a critical need to develop a more efficient, accurate, and stable numerical method specifically designed for solving such problems. The purpose of this study is to employ the WMIGM to solve linear singularly perturbed two-point boundary value problems (see Eq. (1)) based on special segmented equidistant (Shishkin) nodes. A coarse mesh is utilized in the smooth region, and a fine mesh is applied in the boundary layer. Compared with other meshfree methods, our WMIGM approach simplifies the imposition of essential boundary conditions due to its interpolation property. Additionally, we present error estimates of the algorithm, even in the absence of analytic expressions for the shape functions. Test problems are then solved using the WMIGM over modified Shishkin nodes.

This paper is organized as follows. In Section 2, we review the construction of wavelet multiresolution interpolations and some properties of shape functions. In Section 3, we introduce the WMIGM scheme for solving linear singularly perturbed boundary value problems. The parameter uniform convergence is explained in Section 4, followed by numerical experiments and comparisons with existing methods in Section 5, which illustrate the accuracy and efficiency of the proposed wavelet method. Finally, concluding remarks are provided in Section 6.

2 Wavelet Multiresolution Interpolation

This section reviews the construction of the wavelet multiresolution interpolation approximation and explains several key properties of the wavelet interpolating shape function that was proposed in our previous works [54,55].

We begin with the interpolating wavelet transform [44,56], as applied to the following dyadic grids on the real line:

$$\{x_{j,k} \in \mathbf{R} : x_{j,k} = a_0 + 2^{-j}kh_0, k \in \mathbf{Z}\}, \quad (2)$$

where $x_{j,k}$ are the grid points, a_0 is a real number, j is the decomposition level, and h_0 is the spatial step with $j=0$. By using the linear superposition of the interpolating wavelet transform, a continuous function $f(x) \in L^2(\mathbf{R})$ of the form

$$f(x) \approx P_j^{\mathbf{R}} f(x) = \sum_{k \in \mathbf{Z}} f(x_{j,k}) \phi_{j,k}^{\mathbf{R}}(x), \quad (3)$$

is yielded, where $\phi_{j,k}^{\mathbf{R}}(x) = \phi_{0,0}^{\mathbf{R}}[2^j(x - a_0) + x_{0,-k}]$ is the scaling function sampled at point $x_{j,k}$.

Next, we focus on the interpolating wavelet transform construction for interval $[a, b]$ on a set of dyadic grids:

$$\{x_{j,k} \in [a, b] : x_{j,k} = a + 2^{-j}kh_0, k = 0, 1, 2, \dots, n_j\}, \quad (4)$$

where $h_0 = (b - a)/n_0$ is the spatial step with $j=0$, and $n_j = 2^j n_0$ is the number of grids at the level of resolution j , which satisfies $n_0 \geq \gamma$.

By applying Eq. (3) to approximate a continuous function $f(x) \in L^2(\mathbf{R})$ on the interval $[a, b]$, we obtain

$$f(x) \approx P_j^{[a,b]} f(x) = \sum_{k \in \mathbf{Z}} f(x_{j,k}) \phi_{j,k}^{\mathbf{R}}(x) \text{ for } x \in [a, b]. \quad (5)$$

Based on the compact support of the scaling function $\phi_{j,k}^{\mathbf{R}}(x)$, Eq. (5) can be rewritten as

$$f(x) \approx P_j^{[a,b]} f(x) = \sum_{k=1-\gamma}^{n_j+\gamma-1} f(x_{j,k}) \phi_{j,k}^{\mathbf{R}}(x). \quad (6)$$

It can be seen from Eq. (6) that we require the values of $\bar{f}(x)$ at some external auxiliary points located outside the interval $[a, b]$. Following the work of Donoho [56], the unknown values of $f(x_{j,k})$ for $k < 0$ or $k > n_j$ are obtained with the Lagrange interpolation polynomial of degree γ . It follows that we may define a new function $\bar{f}(x)$ such that

$$\bar{f}(x) = \begin{cases} \sum_{k=0}^{\gamma-1} L_{j,k}^a(x) f(x_{j,k}), & x \in [x_{j,1-\gamma}, a) \\ f(x), & x \in [a, b] \\ \sum_{k=n_j-\gamma+1}^{n_j} L_{j,k}^b(x) f(x_{j,k}), & x \in (b, x_{j,n_j+\gamma-1}] \end{cases}, \quad (7)$$

in which

$$L_{j,k}^a(x) = \prod_{\substack{i=0 \\ i \neq k}}^{\gamma-1} \frac{x - x_{j,i}}{x_{j,k} - x_{j,i}}, \quad L_{j,k}^b(x) = \prod_{i=n_j-\gamma+1, i \neq k}^{n_j} \frac{x - x_{j,i}}{x_{j,k} - x_{j,i}}. \quad (8)$$

Substituting Eq. (7) into Eq. (6), we obtain

$$P_j^{[a,b]} f(x) = \sum_{k=0}^{n_j} f(x_{j,k}) \phi_{j,k}^{[a,b]}(x), \quad (9)$$

where the modified wavelet scaling function $\phi_{j,k}^{[a,b]}(x)$ is given by

$$\phi_{j,k}^{[a,b]}(x) = \begin{cases} \phi_{j,k}^{\mathbf{R}}(x) + \sum_{i=1-\gamma}^{-1} L_{j,k}^a(x_{j,i}) \phi_{j,i}^{\mathbf{R}}(x), & k \in [0, \gamma - 1] \\ \phi_{j,k}^{\mathbf{R}}(x), & k \in [\gamma, n_j - \gamma] \\ \phi_{j,k}^{\mathbf{R}}(x) + \sum_{i=n_j+1}^{n_j+\gamma-1} L_{j,k}^b(x_{j,i}) \phi_{j,i}^{\mathbf{R}}(x), & k \in [n_j - \gamma + 1, n_j] \end{cases}. \quad (10)$$

Lemma 2.1 ([54,56]): The modified scaling function $\phi_{j,k}^{[a,b]}(x)$ has the following important properties:

- Compact support: $\phi_{j,k}^{[a,b]}(x) = 0$ for $x \notin [x_{j,\alpha}, x_{j,\beta}]$, where $\alpha = \max\{0, k - \gamma + 1\}$, $\beta = \min\{k + \gamma - 1, n_j\}$;
- Interpolation: $\phi_{j,k}^{[a,b]}(x_{j,l}) = \delta_{k,l}$;
- Polynomial reproduction: $\sum_{k=0}^{n_j} (x_{j,k})^i \phi_{j,k}^{[a,b]}(x) = x^i$ for $i = 0, 1, \dots, \gamma - 1$.

Notice that the grid points in $V_j^{[a,b]}$ are regularly spaced. We next introduce multiresolution interpolation [54,55]:

$$P_{j_0}^{J,[a,b]} f(x) = \sum_{k=0}^N f(x_k) \Theta_{J,k}^{[a,b]}(x), \tag{11}$$

where $N+1$ is the total number of nodes in $[a, b]$, and the wavelet multiresolution interpolating shape function $\Theta_{J,k}^{[a,b]}(x)$ can be obtained using the following recurrence relation:

$$\Theta_{J,k}^{[a,b]}(x) = \phi_k^{[a,b]}(x) - \sum_{j=\rho(x_k, j_0)}^{J-1} \sum_{l \in \mathcal{M}_j} \Theta_{j,k}^{[a,b]}(x_l) \phi_l^{[a,b]}(x), \tag{12}$$

with the following initial condition:

$$\Theta_{j_1, k}^{[a,b]}(x) = \begin{cases} \phi_k^{[a,b]}(x), & \rho(x_k, j_0) = j_1 \\ 0, & \rho(x_k, j_0) > j_1 \end{cases}. \tag{13}$$

In Eq. (13), the function $\rho(x_k, j_0)$ returns an integer with $\rho(x_k, j_0) \geq j_0$ such that $k(x) = 2^{\rho(x_k, j_0)}(x - a)/h_0$ is an integer. For any point x_k , we have $x_k = x_{\rho(x_k, j_0), k(x_k)}$ and $\phi_k^{[a,b]}(x) = \phi_{\rho(x_k, j_0), k(x_k)}^{[a,b]}(x)$. \mathcal{M}_j is the set of all nodes x_k with $\rho(x_k, j_0) = j + 1$.

Lemma 2.2 ([54,55]): The wavelet multiresolution interpolating shape function $\Theta_{J,k}^{[a,b]}(x)$ has the following important properties:

- Interpolation: $\Theta_{J,k}^{[a,b]}(x_l) = \delta_{k,l}$;
- Polynomial reproduction: $\sum_{k=0}^N (x_k)^i \Theta_{J,k}^{[a,b]}(x) = x^i$ for $i = 0, 1, \dots, \gamma - 1$.

Definition 2.1: $V_{j_0}^{J,[a,b]}$ is the set of functions $f(x)$ such that every $f(x) \in V_{j_0}^{J,[a,b]}$ has the following representation:

$$f(x) = \sum_{k=0}^N f(x_k) \Theta_{J,k}^{[a,b]}(x). \tag{14}$$

Lemma 2.3 ([56]): For function $f(x) \in L^\infty([a, b])$, the error between $f(x)$ and $P_{j_0}^{J,[a,b]} f(x)$ can be estimated as

$$\|f(x) - P_{j_0}^{J,[a,b]} f(x)\|_\infty \leq C_1 N^{-\gamma}, \tag{15}$$

where C_1 is a constant, depending on the derivatives of $\Theta_{J,k}^{[a,b]}(x)$ and $f(x)$.

3 Description of the WMIGM

In this section, we formulate the WMIGM for singularly perturbed boundary value problems on Shishkin nodes [19].

3.1 Node Generation

We first divide the computational domain $[0, 1]$ into two subintervals each for left- and right-side boundary layer problems: the fine part $[0, \sigma]$, the crude part $[\sigma, 1]$, and the crude part $[0, 1 - \sigma]$, the fine part $[1 - \sigma, 1]$, respectively. The transition parameter is defined by $\sigma = \min\{1/2, \alpha \varepsilon \ln(N)/|p|\}$, where $\alpha \geq \gamma$, and $N \in \mathbb{N}$ is the total number of grids. We consider that the number of grid points in

each subdomain is equal and that they are uniformly divided; thus the step of the grid in the rough region is $h_S = 2(1 - \sigma)/N$, and that in the fine region is $h_E = 2\sigma/N$. Following the recurrence relation of Eq. (12), we have

$$h_S = 2^J h_E, \quad (16)$$

in which J is an integer.

In the subsequent calculations, we set $\sigma = 1/(2^J + 1)$, in which $J = \max\{0, \lceil -\log_2(\varepsilon) - \alpha \rceil\}$ is an integer, and α is an integer. Thus, we have

$$\varepsilon^{-1} \leq 2^{J+\alpha}. \quad (17)$$

We then evenly arrange the nodes into two subintervals:

$$x_k = \begin{cases} 2^{-J}kh, & \text{if } k = 0, 1, \dots, N/2 \\ \sigma + (k - N/2)h, & \text{if } k = N/2 + 1, \dots, N \end{cases} \quad (18)$$

for left-side boundary layer problems, and

$$x_k = \begin{cases} kh, & \text{if } k = 0, 1, \dots, N/2 \\ \sigma + 2^{-J}kh, & \text{if } k = N/2 + 1, \dots, N \end{cases} \quad (19)$$

for right-side boundary layer problems.

After the nodes are generated, we use the iterative formula in Eq. (12) to obtain the wavelet multiresolution interpolating shape functions. Then, the approximation solution of $u(x)$ can be calculated with Eq. (11).

3.2 WMIGM for Singularly Perturbed Boundary Value Problems

The variational form of Eq. (1) is $u(x) \in H_0^1(0, 1)$, such that

$$-\varepsilon \int_0^1 u'v' dx + a \int_0^1 u'v dx + b \int_0^1 uv dx = \int_0^1 f v dx \quad \text{for all } v \in H_0^1(0, 1). \quad (20)$$

Then, we replace the infinite dimensional space, $H_0^1(0, 1)$, with the wavelet multiresolution interpolation space, $V_{j_0}^{J,[a,b]}$, and obtain the WMIGM:

$$-\varepsilon \int_0^1 u_h'v' dx + a \int_0^1 u_h'v dx + b \int_0^1 u_h v dx = \int_0^1 f_h v dx \quad \text{for all } v \in V_{j_0}^{J,[0,1]}, \quad (21)$$

where $u_h(x) \in V_{j_0}^{J,[a,b]}$, and $v(x) = \Theta_{J,l}^{[a,b]}(x)$ is selected for $l = 1, 2, 3, \dots, N - 1$.

Using Eq. (11), the approximate solutions for $u_h(x)$ and $f_h(x)$ can be represented by

$$\begin{cases} u_h(x) = \sum_{k=0}^N u_h(x_k) \Theta_{J,k}^{[0,1]}(x) \\ f_h(x) = \sum_{k=0}^N f_h(x_k) \Theta_{J,k}^{[0,1]}(x) \end{cases} \quad (22)$$

Substituting Eq. (22) into Eq. (21), we obtain the following matrix form:

$$-\varepsilon \mathbf{A}_0 \mathbf{u}_h + a \mathbf{A}_1 \mathbf{u}_h + b \mathbf{A}_2 \mathbf{u}_h = \mathbf{A}_2 \mathbf{f}_h, \quad (23)$$

in which the matrices are $\mathbf{A}_0 = \{A_{0,k_1,l} = \Gamma_{J,J,k_1,l}^{\ominus,1,1,[0,1]}\}$, $\mathbf{A}_1 = \{A_{1,k_1,l} = \Gamma_{J,J,k_1,l}^{\ominus,0,1,[0,1]}\}$, and $\mathbf{A}_2 = \{A_{2,k_1,l} = \Gamma_{J,J,k_1,l}^{\ominus,0,0,[0,1]}\}$. The vectors are $\mathbf{u}_h = \{u_{h,l,1} = u_h(x_l)\}$ and $\mathbf{f}_h = \{f_{h,l,1} = f_h(x_l)\}$ for $k, l = 0, 1, 2, \dots, N$ and $k_1, l_1 =$

1, 2, 3, . . . , N − 1, respectively. Here, the connection coefficients, $\Gamma_{J,J,k,l}^{\Theta,n,m,[0,1]} = \int_0^1 \Theta_{J,k}^{(n),[0,1]}(x) \Theta_{J,l}^{(m),[0,1]}(x) dx$, can be precisely obtained [54].

Using this process, we can obtain the WMIGM solutions by solving Eq. (23).

4 Error Analysis

In this section, we provide the WMIGM’s error estimate, which relies on the modified Shishkin nodes. In the following analysis, we assume that $\varepsilon N \geq 2^{1-\alpha}$ to ensure that $N \geq 2^{J+1}$ holds. The solution of Eq. (1) can be decomposed into $u = S + E$, in which S is the smooth component and E is the boundary layer component [12,21,57,58], where

$$|S^{(k)}(x)| \leq C, \quad |E^{(k)}(x)| \leq C\varepsilon^{-k} e^{-\beta x/\varepsilon} \text{ for } k = 0, 1, \dots, \gamma \text{ and } x \in [0, 1]. \tag{24}$$

Based on the properties of the wavelet multiresolution interpolating shape functions introduced in the previous Section 2, we have the following interpolation error estimates.

Lemma 4.1: Let $P_{j_0}^J u$ be the wavelet multiresolution interpolant of $u(x)$ on the modified Shishkin nodes. Thus, we obtain the properties for

$$\|u - P_{j_0}^J u\|_{L^\infty(\Omega)} \leq CN^{-\gamma}, \tag{25}$$

$$\|u - P_{j_0}^J u\|_\varepsilon \leq CN^{1-\gamma}, \tag{26}$$

where C is independent of N and ε , and the energy norm is defined as

$$\|v\|_\varepsilon := \{\varepsilon\|v'\|_{L^2}^2 - q\|v\|_{L^2}^2\}^{1/2} \quad \forall v \in H^1(\Omega). \tag{27}$$

Proof: Using a Taylor expansion at x_i , the interpolation error of $|S(x) - P_{j_0}^{J[a,b]} S(x)|$ for $x \in [x_i, x_{i+1}]$ can be rewritten as

$$|S(x) - P_{j_0}^J S(x)| = \frac{S^{(\gamma)}(\zeta)}{\gamma!} (x - x_i)^\gamma, \tag{28}$$

where $\zeta \in [x_i, x]$. From Eq. (24), we get

$$|S(x) - P_{j_0}^J S(x)| \leq Ch_S^\gamma \leq CN^{-\gamma}. \tag{29}$$

Then, from Eqs. (17) and (24), on the boundary layer part, we have

$$\begin{aligned} |E - P_{j_0}^J E(x)| &= \frac{E^{(\gamma)}(\zeta)}{\gamma!} (x - x_i)^\gamma \\ &\leq Ch_E^\gamma \varepsilon^{-\gamma} \leq CN^{-\gamma} \left(\frac{2}{2^J + 1} \varepsilon^{-1}\right)^\gamma \leq CN^{-\gamma} \left(\frac{2^{J+\alpha+1}}{2^J + 1}\right)^\gamma. \\ &\leq CN^{-\gamma} \end{aligned} \tag{30}$$

Obviously, Eq. (25) can be easily demonstrated through Eqs. (28) and (30).

Thus, it remains to prove the estimate Eq. (26). From Eq. (24), we get

$$\begin{aligned} \|(u - P_{j_0}^J u)\|_{L^2(\Omega_S)} &\leq Ch_S^{\gamma-1} \|E^{(k)}(x)\|_{L^2(\Omega_S)} \leq Ch_S^{\gamma-1} (1 - \sigma) \\ &\leq Ch_S^{\gamma-1} \leq CN^{1-\gamma} \end{aligned} \tag{31}$$

$$\begin{aligned} \|(u - P_{j_0}^J u)'\|_{L^2(\Omega_E)} &\leq Ch_E^{\gamma-1} \|E^{(k)}(x)\|_{L^2(\Omega_E)} \leq Ch_E^{\gamma-1} (\sigma \varepsilon^{-2\gamma})^{1/2} \\ &\leq Ch_E^{\gamma-1} (2^\alpha \varepsilon^{1-2\gamma})^{1/2} \leq C \varepsilon^{-1/2} N^{1-\gamma} \end{aligned} \quad (32)$$

The estimation of Eq. (26) can then be derived immediately.

Theorem 4.1: Let u be the solution of Eq. (1) and $u^N \in V_{j_0}^{J,[a,b]}$ be the WMIGM solution of Eq. (23). Thus, we have

$$\|u - u^N\|_\varepsilon \leq CN^{1-\gamma}, \text{ for } N\varepsilon \geq 2^{1-\alpha}, \quad (33)$$

in which C is independent of N and ε .

Proof: Let $\xi := P_{j_0}^J u - u^N$. Applying the Galerkin orthogonality, we get

$$\begin{aligned} \|\xi\|_\varepsilon^2 &= \varepsilon \|(\xi)'\|_{L^2(\Omega)}^2 - q \|\xi\|_{L^2(\Omega)}^2 \\ &= \varepsilon \left| \int_0^1 \xi' \xi' dx \right| - q \left| \int_0^1 \xi \xi dx \right| \\ &\leq \varepsilon \left| \int_0^1 (P_{j_0}^J u - u)' \xi' dx \right| + \left| -p \int_0^1 (P_{j_0}^J u - u)' \xi dx \right| - q \left| \int_0^1 (P_{j_0}^J u - u) \xi dx \right| \\ &=: \text{I} + \text{II} + \text{III} \end{aligned} \quad (34)$$

Owing to the Hölder inequalities and Eq. (26) of Lemma 4.1, it holds that

$$\text{I} + \text{III} \leq C \|P_{j_0}^J u - u\|_\varepsilon \|\xi\|_\varepsilon \leq CN^{1-\gamma} \|\xi\|_\varepsilon. \quad (35)$$

With the aid of integrating by parts and the Cauchy-Schwarz inequality, we observe that

$$\begin{aligned} \text{II} &= -p \int_0^1 (P_{j_0}^J u - u)' \xi dx = p \int_0^1 (P_{j_0}^J u - u) \xi' dx \\ &\leq C \|u - P_{j_0}^J u\|_{L^2(\Omega)} \|\xi\|_{L^2(\Omega)} \leq CN^{-\gamma} \|\xi\|_{L^2(\Omega)}. \\ &\leq CN^{-\gamma} \|\xi\|_\varepsilon \end{aligned} \quad (36)$$

As a result,

$$\|\xi\|_\varepsilon \leq CN^{1-\gamma}. \quad (37)$$

Hence, $u - u^N$ can be bounded by

$$\|u - u^N\|_\varepsilon \leq \|u - P_{j_0}^J u\|_\varepsilon + \|P_{j_0}^J u - u^N\|_\varepsilon \leq CN^{1-\gamma}, \quad (38)$$

which is the required result.

5 Numerical Results

In this section, we applied the WMIGM to four examples to evaluate its numerical accuracy. We considered two grid points: uniform node points using the wavelet interpolation Galerkin method (WIGM) and refined local grid points using the WMIGM, as specified in Section 3. If not otherwise specified, $\gamma = 6$ and $\alpha = 3$.

To estimate the accuracy of the solutions, the maximum absolute and ε -uniform errors at the grid points are taken as

$$\begin{aligned} E_{\max}(N) &= \max_{0 \leq i \leq N} |u_e(x_i) - u_h(x_i)| \\ E_\varepsilon(N) &= \left\{ \sum_{i=0}^N \varepsilon [u'_e(x_i) - u'_h(x_i)]^2 - q [u_e(x_i) - u_h(x_i)]^2 \right\}^{1/2}, \end{aligned} \quad (39)$$

and the numerical rates of convergence are

$$R = \log_2[E_{\max,\varepsilon}(N)/E_{\max,\varepsilon}(2N)]. \quad (40)$$

All numerical results were conducted on an AMD Ryzen 7 3700X CPU @ 3.20 GHz with 64 GB RAM in MATLAB.

5.1 Test Problem 1: Left-Side Boundary Layer Problem

We begin our numerical cases with the following left-side boundary layer problem [6–7,59,60]:

$$\varepsilon u'' + u' = 1 + 2x. \quad (41)$$

The boundary conditions are extracted from the exact solution as

$$u(x) = x(x + 1 - 2\varepsilon) + (2\varepsilon - 1)(1 - e^{-x/\varepsilon})/(1 - e^{-1/\varepsilon}). \quad (42)$$

The absolute errors obtained by the proposed WIGM with $N = 100$ for different values of ε are presented in Fig. 1. The numerical results show that the errors are mainly located near the left-side boundary layer, and they increase with the decrease of ε . In Table 1, we list the maximum absolute errors and computational orders of convergence on uniform points using the WIGM and non-uniform points using the WMIGM for different values of ε and grid points N with $\gamma = 6$. From Table 1, we find that the numerical solutions obtained by the WMIGM are much better than those computed by the WIGM, especially for $\varepsilon \rightarrow 0$. In particular, WMIGM using 256 grid points exhibits slightly better accuracy than the WIGM using 512 nodes for $\varepsilon = 2^{-5}$ and $\varepsilon = 2^{-6}$. Therefore, solution accuracy can be improved by adding local nodes in the boundary layer. Moreover, a comparison of the numerical errors obtained by the WIGM, the WMIGM, the quintic B-spline method (QBSM) with Shishkin mesh [6], and the novel optimal B-spline (NOBS) technique with Shishkin mesh [7] is also illustrated in Table 1. There, it can be seen that for most cases, the WMIGM is more accurate than the QBSM and the NOBS, given the same number of grid points for most cases listed. The numerical solutions obtained by the WIGM and the WMIGM are shown in Fig. 2 with the corresponding exact solution for $\varepsilon = 2^{-9}$. Note that the WMIGM with $N = 64$ can achieve nearly the same accuracy as the analytical solution, whereas the WIGM does not converge at small ε values. To visualize the convergence ratio of the proposed algorithm, Fig. 3 displays the error norm as a function of the number of grid points with $\varepsilon = 2^{-7}$. It can be seen that the proposed WMIGM's convergence rate of $E_\varepsilon(N)$ is approximately $\gamma - 1$ for $N\varepsilon \geq 2^{-2}$, which is consistent with the previous error analysis. Moreover, the curves visually demonstrate that our results are better than the QBSM and the NOBS, and the numerical convergence rate of the maximum error E_{\max} is approximately γ . Notably, the results of the WMIGM with $\gamma = 6$ are quite bad for $N = 32$, as shown in Table 1. We conclude that is due to the support domains of the shape functions will become larger as γ increases. Thus, we need more sampling points to capture the local large gradient information for a large γ . We can see that this phenomenon does not occur when $\gamma = 4$.

5.2 Test Problem 2: Left-Side Boundary Layer Problem

We next consider a source-free singularly perturbed problem as described in [3,10,60–62]:

$$\varepsilon u'' + u' - u = 0, \quad (43)$$

whose analytical solution is given by

$$u(x) = \frac{(e^{m_2} - 1)e^{m_1 x} + (1 - e^{m_1})e^{m_2 x}}{e^{m_2} - e^{m_1}}, \tag{44}$$

in which $m_1 = (-1 + \sqrt{1 + 4\epsilon})/(2\epsilon)$ and $m_2 = (-1 - \sqrt{1 + 4\epsilon})/(2\epsilon)$. The solution $u(x)$ satisfies the boundary conditions of $u(0) = 1$ and $u(1) = 1$.

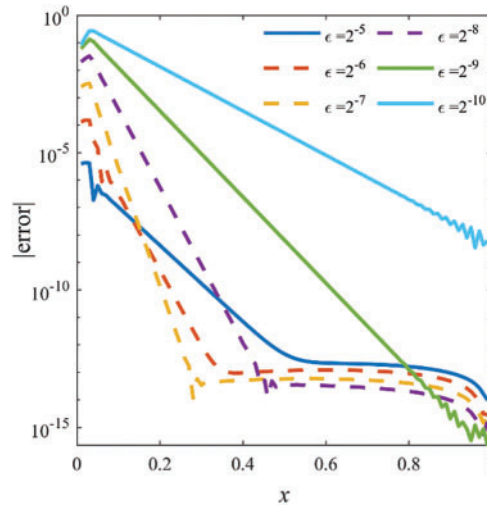


Figure 1: Absolute errors of WIGM for Example 1 with $N = 100$

Table 1: Maximum absolute errors and convergence rate of Example 1 for different values of ϵ and N

N	Method	$\epsilon = 2^{-3}$		$\epsilon = 2^{-4}$		$\epsilon = 2^{-5}$		$\epsilon = 2^{-6}$		$\epsilon = 2^{-7}$	
		E_{max}	R								
16	WIGM	3.53E-05		1.06E-03		1.53E-02		8.65E-02			
	WMIGM	3.53E-05		1.68E-04		4.47E-03		1.56E-02			
32	WIGM	9.04E-07	5.29	4.12E-05	4.69	1.14E-03	3.75	1.58E-02	2.46	8.75E-02	
	WMIGM	9.04E-07	5.29	5.01E-06	5.06	4.09E-05	6.77	5.11E-03	1.61	1.60E-02	
64	WIGM	1.82E-08	5.64	1.05E-06	5.29	4.41E-05	4.69	1.17E-03	3.75	1.60E-02	2.45
	WMIGM	1.82E-08	5.64	1.09E-07	5.52	6.79E-07	5.91	3.96E-05	7.01	5.48E-03	1.55
	NOBS [7]	7.43E-10		5.21E-08		2.91E-06		1.15E-04		1.55E-03	
128	QBSM [6]	9.27E-08		1.71E-06		2.75E-05		3.78E-04		5.38E-03	
	WIGM	3.22E-10	5.82	2.12E-08	5.64	1.13E-06	5.29	4.56E-05	4.69	1.19E-03	3.75
	WMIGM	3.22E-10	5.82	2.02E-09	5.76	1.25E-08	5.77	6.31E-07	5.97	3.79E-05	7.18
	NOBS [7]	1.18E-11	5.97	8.71E-10	5.90	5.58E-08	5.70	3.00E-06	5.26	1.17E-04	3.73
256	QBSM [6]	5.81E-09	3.99	1.09E-07	3.98	1.83E-06	3.91	2.85E-05	3.73	3.84E-04	3.81
	WIGM	5.46E-12	5.88	3.76E-10	5.82	2.27E-08	5.64	1.17E-06	5.29	4.63E-05	4.69
	WMIGM	5.46E-12	5.88	3.45E-11	5.87	2.21E-10	5.82	1.16E-08	5.77	5.87E-07	6.01
	NOBS [7]	1.86E-13	5.99	1.39E-11	5.97	9.33E-10	5.90	5.77E-08	5.7	3.05E-06	5.26
	QBSM [6]	3.64E-10	4.00	6.81E-09	3.99	1.16E-07	3.98	1.89E-06	3.91	2.89E-05	3.73

(Continued)

Table 1 (continued)

N	Method	$\varepsilon = 2^{-3}$		$\varepsilon = 2^{-4}$		$\varepsilon = 2^{-5}$		$\varepsilon = 2^{-6}$		$\varepsilon = 2^{-7}$	
		E_{max}	R								
512	WIGM	-	-	1.11E-11	5.08	4.04E-10	5.81	2.35E-08	5.64	1.19E-06	5.29
	WMIGM	-	-	-	-	3.68E-12	5.91	2.07E-10	5.81	1.08E-08	5.77
	NOBS [7]	2.91E-15	6.00	2.18E-13	5.99	1.45E-11	5.97	9.64E-10	5.90	5.86E-08	5.70
	QBSM [6]	2.27E-11	4.00	4.26E-10	4.00	7.30E-09	3.99	1.20E-07	3.98	1.92E-06	3.91
1024	WIGM	-	-	-	-	-	-	4.18E-10	5.81	2.38E-08	5.64
	WMIGM	-	-	-	-	-	-	-	-	1.91E-10	5.81
	NOBS [7]	4.54E-17	6.00	3.41E-15	6.00	2.33E-13	5.99	1.55E-11	5.96	9.80E-10	5.90
	QBSM [6]	1.35E-12	4.07	2.65E-11	4.01	4.57E-10	4.00	7.54E-09	3.99	1.22E-07	3.98

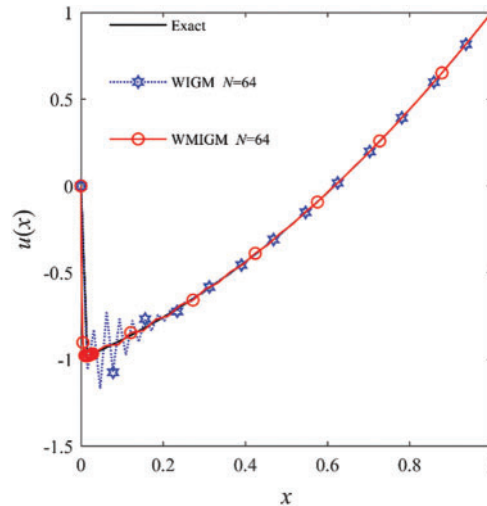


Figure 2: The comparison of the numerical solutions with the exact solution for Example 1 with $\varepsilon = 2^{-9}$

Table 2 shows the comparison of the maximum absolute errors between the QBSM with Shishkin mesh [6], the NOBS with Shishkin mesh [7], and the proposed WIGM and WMIGM with respect to the number of grid points for various values of ε . It can be seen that the number of grid points must be increased to obtain a reliable numerical solution as ε decreases. We can see from Fig. 4 that the method of locally enhancing nodes at the boundary layer using the WMIGM performs significantly better than the method utilizing uniform nodes using the WIGM when the same number of nodes is used. The latter has obvious spurious oscillations in the boundary layer region. The error norms as a function of the number of nodes are illustrated in Fig. 5, where $\varepsilon = 2^{-7}$. We have shown that the WMIGM is much more accurate than the QBSM [6] and the NOBS [7], and the order of accuracy of the WMIGM with ε -uniform error norm is approximately $\gamma - 1$. Additionally, the maximum absolute error convergence rate of the WMIGM with $\gamma = 6$ is approximately 6.18, which is larger than that of other algorithms.

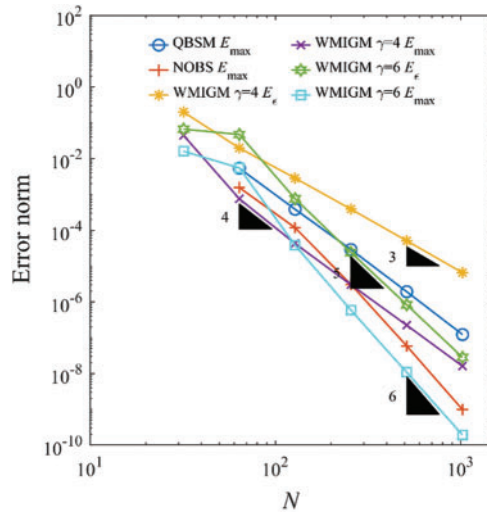


Figure 3: Error norm as a function of the number of grid points for Example 1 with $\varepsilon = 2^{-7}$

Table 2: Maximum absolute errors and convergence rate of Example 2 for different values of ε and N

N	Method	$\varepsilon = 2^{-3}$		$\varepsilon = 2^{-4}$		$\varepsilon = 2^{-5}$		$\varepsilon = 2^{-6}$		$\varepsilon = 2^{-7}$	
		E_{max}	R								
16	WIGM	4.71E-05		9.30E-04		1.09E-02		5.64E-02			
	WMIGM	4.71E-05		1.53E-04		2.98E-03		1.02E-02			
32	WIGM	1.28E-06	5.21	3.82E-05	4.61	8.48E-04	3.68	1.06E-02	2.41	5.63E-02	
	WMIGM	1.28E-06	5.21	4.74E-06	5.01	2.65E-05	6.81	3.32E-03	1.62	1.04E-02	
64	WIGM	2.64E-08	5.59	1.01E-06	5.25	3.39E-05	4.65	8.07E-04	3.71	1.04E-02	2.43
	WMIGM	2.64E-08	5.59	1.06E-07	5.49	4.38E-07	5.92	2.51E-05	7.04	3.51E-03	1.57
	NOBS [7]	9.76E-10		4.73E-08		2.16E-06		5.10E-05		1.03E-03	
	QBSM [6]	1.02E-07		1.42E-06		1.99E-05		2.55E-04		3.55E-03	
128	WIGM	4.75E-10	5.80	2.05E-08	5.61	8.81E-07	5.27	3.18E-05	4.67	7.87E-04	3.73
	WMIGM	4.75E-10	5.80	1.97E-09	5.74	8.08E-09	5.76	3.98E-07	5.98	2.39E-05	7.20
	NOBS [7]	1.57E-11	5.96	7.97E-10	5.89	4.24E-08	5.90	2.06E-06	4.63	7.66E-05	3.74
	QBSM [6]	6.41E-09	3.99	9.01E-08	3.98	1.33E-06	3.91	1.92E-05	3.73	2.50E-04	3.82
256	WIGM	1.19E-11	5.32	3.67E-10	5.81	1.78E-08	5.63	8.20E-07	5.28	3.08E-05	4.68
	WMIGM	1.19E-11	5.32	3.35E-11	5.88	1.45E-10	5.80	7.33E-09	5.76	3.70E-07	6.02
	NOBS [7]	2.47E-13	5.99	1.27E-11	5.97	7.11E-10	5.97	4.00E-08	5.69	2.01E-06	5.25
	QBSM [6]	4.01E-10	4.00	5.67E-09	3.99	8.43E-08	3.98	1.28E-06	3.91	1.89E-05	3.73
512	WIGM	-	-	-	-	3.16E-10	5.82	1.66E-08	5.63	7.91E-07	5.28
	WMIGM	-	-	-	-	8.36E-12	4.12	1.33E-10	5.78	6.78E-09	5.77
	NOBS [7]	3.86E-15	6.00	2.00E-13	5.99	1.13E-11	5.97	6.70E-10	5.90	3.88E-08	5.70
	QBSM [6]	2.51E-11	4.00	3.55E-10	4.00	5.29E-09	3.99	8.14E-08	3.98	1.26E-06	3.91
1024	WIGM	-	-	-	-	-	-	2.91E-10	5.83	1.59E-08	5.63
	WMIGM	-	-	-	-	-	-	-	-	1.26E-10	5.75

(Continued)

Table 2 (continued)

N	Method	$\varepsilon = 2^{-3}$		$\varepsilon = 2^{-4}$		$\varepsilon = 2^{-5}$		$\varepsilon = 2^{-6}$		$\varepsilon = 2^{-7}$	
		E_{max}	R								
	NOBS [7]	6.03E-17	6.00	3.13E-15	6.00	1.78E-13	5.99	1.07E-11	5.97	6.49E-10	5.90
	QBSM [6]	1.74E-12	3.85	2.22E-11	4.00	3.31E-10	4.00	5.11E-09	3.99	7.99E-08	3.98

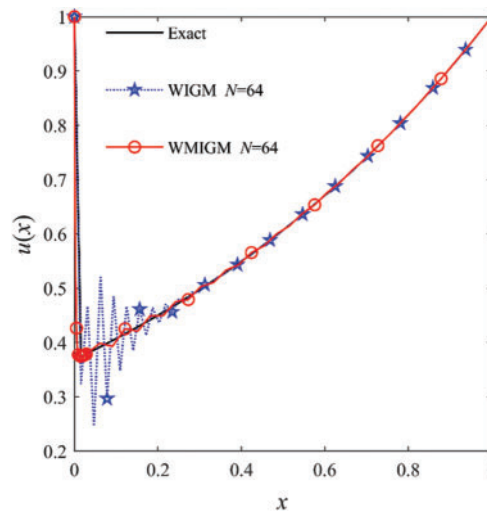


Figure 4: The comparison of the numerical solutions with the exact solution for Example 2 with $\varepsilon = 2^{-9}$

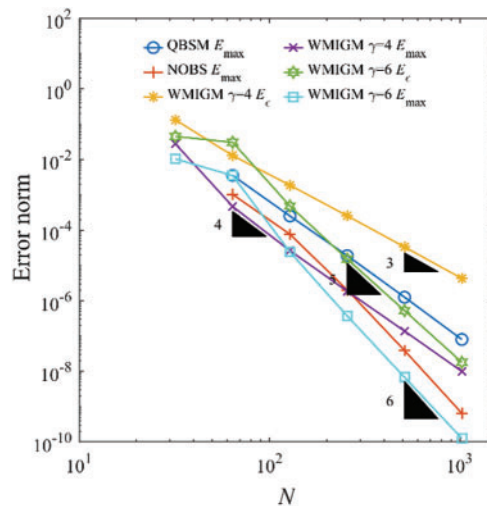


Figure 5: Error norm as a function of the number of grid points for Example 2 with $\varepsilon = 2^{-7}$

5.3 Test Problem 3: Right-Side Boundary Layer Problem

We next consider the right-side boundary layer problem [6,13,63–65]:

$$\epsilon u'' - u' = 0, \tag{45}$$

with boundary conditions of $u(0) = 1$ and $u(1) = 0$. The exact solution of this problem is

$$u(x) = \frac{e^{(x-1)/\epsilon} - 1}{e^{-1/\epsilon} - 1}. \tag{46}$$

Fig. 6 displays the absolute errors for the uniform mesh with different values of ϵ , and we observe that the errors are mainly located in the right-side boundary layer region. The obtained maximum absolute errors and computational orders of convergence are presented in comparison with the existing QBSM method [6] in Table 3 for different values of ϵ and N . From this table, we can conclude that our numerical solutions obtained by the WMIGM are in good agreement with the exact values and are more accurate than the QBSM, which is a fourth-order scheme [6]. It can also be seen from Fig. 7 that the non-physical oscillation can be greatly reduced by locally increasing the number of nodes in the boundary layer.

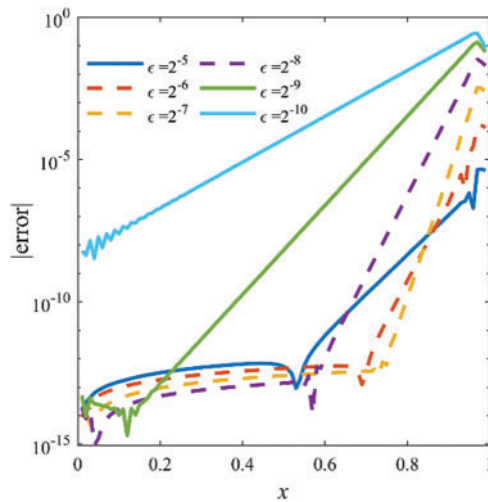


Figure 6: Absolute errors of WIGM for Example 3 with $N = 100$

Table 3: Maximum absolute errors and convergence rate of Example 3 for different values of ϵ and N

N	Method	$\epsilon = 2^{-3}$		$\epsilon = 2^{-4}$		$\epsilon = 2^{-5}$		$\epsilon = 2^{-6}$		$\epsilon = 2^{-7}$	
		E_{max}	R								
16	WIGM	4.71E-05		1.21E-03		1.63E-02		8.92E-02			
	WMIGM	4.71E-05		1.92E-04		4.70E-03		1.57E-02			
32	WIGM	1.20E-06	5.29	4.70E-05	4.69	1.21E-03	3.75	1.63E-02	2.46	8.89E-02	
	WMIGM	1.20E-06	5.29	5.73E-06	5.06	4.36E-05	6.75	5.27E-03	1.57	1.63E-02	
64	WIGM	2.42E-08	5.64	1.20E-06	5.29	4.70E-05	4.69	1.21E-03	3.75	1.63E-02	2.45
	WMIGM	2.42E-08	5.64	1.25E-07	5.52	7.24E-07	5.91	4.09E-05	7.01	5.57E-03	1.55

(Continued)

Table 3 (continued)

N	Method	$\varepsilon = 2^{-3}$		$\varepsilon = 2^{-4}$		$\varepsilon = 2^{-5}$		$\varepsilon = 2^{-6}$		$\varepsilon = 2^{-7}$	
		E_{max}	R								
128	QBSM [6]	1.24E-07		1.95E-06		2.94E-05		3.40E-05		3.40E-05	
	WIGM	4.31E-10	5.81	2.42E-08	5.64	1.20E-06	5.29	4.70E-05	4.69	1.21E-03	3.75
	WMIGM	4.31E-10	5.81	2.31E-09	5.76	1.33E-08	5.77	6.51E-07	5.97	3.85E-05	7.18
256	QBSM [6]	7.75E-09	3.99	1.24E-07	3.98	1.95E-06	3.91	2.57E-06	3.73	2.67E-06	3.67
	WIGM	2.25E-11	4.26	4.32E-10	5.81	2.42E-08	5.64	1.20E-06	5.29	4.70E-05	4.69
	WMIGM	2.25E-11	4.26	4.02E-11	5.85	2.32E-10	5.84	1.20E-08	5.77	5.96E-07	6.01
512	QBSM [6]	4.85E-10	4.00	7.79E-09	3.99	1.24E-07	3.98	1.90E-07	3.76	2.01E-07	3.74
	WIGM	-	-	-	-	4.34E-10	5.80	2.42E-08	5.64	1.20E-06	5.29
	WMIGM	-	-	-	-	1.36E-11	4.09	2.08E-10	5.85	1.09E-08	5.77
1024	QBSM [6]	3.03E-11	4.00	4.87E-10	4.00	7.79E-09	3.99	1.30E-08	3.87	1.59E-08	3.65
	WIGM	-	-	-	-	-	-	4.39E-10	5.78	2.42E-08	5.64
	WMIGM	-	-	-	-	-	-	2.68E-11	2.96	1.84E-10	5.89
	QBSM [6]	1.76E-12	4.10	3.04E-11	4.00	4.87E-10	4.00	1.00E-09	3.69	1.39E-09	3.81

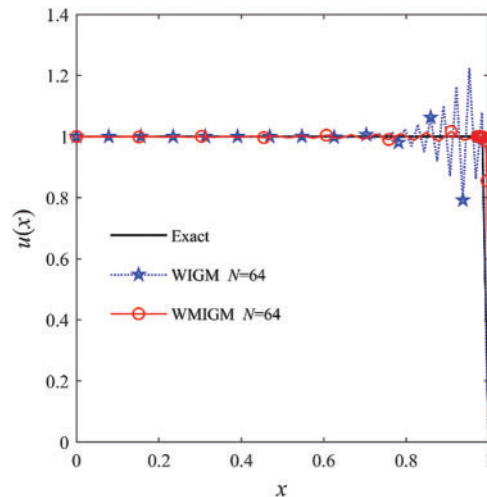


Figure 7: The comparison of the numerical solutions with the exact solution for Example 3 with $\varepsilon = 2^{-9}$

5.4 Test Problem 4: Right-Side Boundary Layer Problem

Finally, we consider the following homogeneous linear singularly perturbed boundary value problem [5,7,63,66,67]:

$$\varepsilon u'' - u' - (1 + \varepsilon)u = 0, \tag{47}$$

with boundary conditions extracted from the exact solution as

$$u(x) = e^{(1+\varepsilon)(x-1)/\varepsilon} + e^{-x}. \tag{48}$$

The maximum absolute errors obtained by the QBSM with Shishkin mesh [6], the NOBS with Shishkin mesh [7], and the proposed WIGM and WMIGM are presented in Table 4. It is evident from this table that WMIGM can achieve more accurate approximate solutions. A comparison of the numerical and analytic solutions with $\varepsilon = 2^{-9}$ is shown in Fig. 8. The accuracy of the present wavelet solution near the right-side boundary layer was improved with the addition of local nodes. Fig. 9 shows that the convergence rate of the proposed WMIGM with $\gamma = 6$ is 6.19, whereas the convergence orders of the QBSM with Shishkin mesh [6] and the NOBS with Shishkin mesh [7] are only 3.81 and 4.89, respectively. Therefore, the WMIGM is significantly more accurate than these previously developed methods.

Table 4: Maximum absolute errors and convergence rate of Example 4 for different values of ε and N

N	Method	$\varepsilon = 2^{-3}$		$\varepsilon = 2^{-4}$		$\varepsilon = 2^{-5}$		$\varepsilon = 2^{-6}$		$\varepsilon = 2^{-7}$	
		E_{max}	R								
16	WIGM	8.40E-05		1.54E-03		1.76E-02		9.01E-02			
	WMIGM	8.40E-05		2.54E-04		4.78E-03		1.63E-02			
32	WIGM	2.29E-06	5.20	6.35E-05	4.60	1.37E-03	3.68	1.69E-02	2.41	8.94E-02	
	WMIGM	2.29E-06	5.20	7.89E-06	5.01	4.27E-05	6.81	5.29E-03	1.62	1.66E-02	
64	WIGM	4.75E-08	5.59	1.68E-06	5.24	5.48E-05	4.64	1.29E-03	3.71	1.66E-02	2.43
	WMIGM	4.75E-08	5.59	1.76E-07	5.49	7.05E-07	5.92	4.01E-05	7.04	5.57E-03	1.57
	NOBS [7]	1.74E-09		7.86E-08		3.50E-06		8.26E-05		7.99E-04	
	QBSM [6]	1.79E-07		2.34E-06		3.21E-05		4.07E-04		4.92E-03	
128	WIGM	8.56E-10	5.79	3.43E-08	5.61	1.42E-06	5.27	5.08E-05	4.67	1.25E-03	3.73
	WMIGM	8.56E-10	5.79	3.29E-09	5.74	1.30E-08	5.76	6.36E-07	5.98	3.80E-05	7.20
	NOBS [7]	2.79E-11	5.96	1.32E-09	5.89	6.85E-08	5.67	3.29E-06	4.65	7.82E-05	3.35
	QBSM [6]	1.12E-08	3.99	1.49E-07	3.98	2.14E-06	3.91	3.07E-05	3.73	3.98E-04	3.63
256	WIGM	1.54E-11	5.80	6.12E-10	5.81	2.89E-08	5.62	1.31E-06	5.28	4.89E-05	4.68
	WMIGM	1.54E-11	5.80	5.60E-11	5.88	2.33E-10	5.80	1.17E-08	5.76	5.87E-07	6.02
	NOBS [7]	4.39E-13	5.99	2.12E-11	5.97	1.15E-09	5.90	6.39E-08	5.69	3.20E-06	4.61
	QBSM [6]	7.02E-10	4.00	9.37E-09	3.99	1.36E-07	3.98	2.05E-06	3.91	3.00E-05	3.73
512	WIGM	-	-	2.74E-11	4.48	5.13E-10	5.82	2.65E-08	5.63	1.26E-06	5.28
	WMIGM	-	-	-	-	9.40E-12	4.63	2.12E-10	5.79	1.08E-08	5.77
	NOBS [7]	6.88E-15	6.00	3.33E-13	5.99	1.83E-11	5.97	1.07E-09	5.90	6.17E-08	5.70
	QBSM [6]	4.39E-11	4.00	5.86E-10	4.00	8.54E-09	3.99	1.30E-07	3.98	2.00E-06	3.91
1024	WIGM	-	-	-	-	5.39E-11	3.25	4.67E-10	5.82	2.53E-08	5.63
	WMIGM	-	-	-	-	-	-	1.35E-11	3.97	1.98E-10	5.76
	NOBS [7]	1.08E-16	6.00	5.20E-15	6.00	2.88E-13	5.99	1.71E-11	5.96	1.03E-09	5.90
	QBSM [6]	2.77E-12	3.98	3.66E-11	4.00	5.35E-10	4.00	8.16E-09	3.99	1.27E-07	3.98

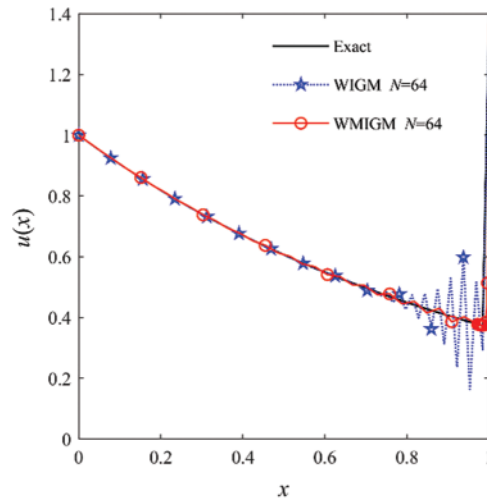


Figure 8: The comparison of the numerical solutions with the exact solution for Example 4 with $\varepsilon = 2^{-9}$

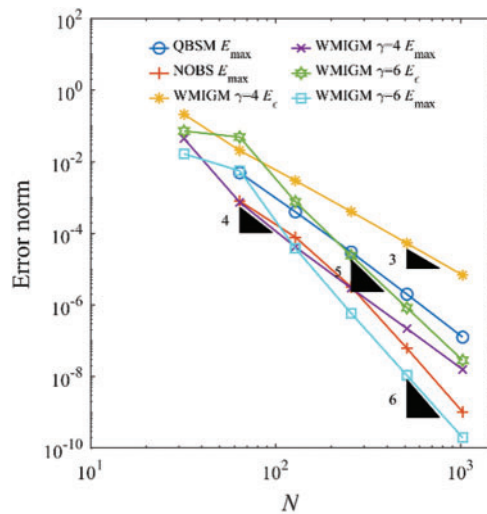


Figure 9: Error norm as a function of the number of grid points for Example 4 with $\varepsilon = 2^{-7}$

6 Conclusion

In this study, we extended the WMIGM to solve linear singularly perturbed boundary value problems with modified Shishkin nodes. The proposed wavelet scheme was verified by comparing the numerical solutions obtained via the QBSM with Shishkin mesh and the NOBS with Shishkin mesh. The numerical results confirm the theoretical analysis and demonstrate that WMIGM has several advantages over existing schemes:

- (1) The accuracy of the WMIGM is significantly better than that of the WIGM. The approximate solutions obtained by the WMIGM exhibit no obvious spurious oscillations near the boundary layer, even as the perturbation parameter approaches zero.

- (2) The WMIGM exhibits greater accuracy than existing schemes, including those of the QBSM and NOBS methods with Shishkin mesh.
- (3) The WMIGM demonstrates a six-order convergence rate and retains a stable convergence order better than that of the QBSM and NOBS methods with the Shishkin mesh.

These advantages indicate the potentially wide application of the WMIGM to simulating problems with local large gradients. Since the proposed WMIGM allows a very flexible nodal distribution, it can be extended to solve other problems with localized steep gradients, such as the steady-state convection diffusion problems, the steady-state heat transfer at high Péclet numbers, and the planar thin plate problems in solid mechanics. Additionally, the combination of the time integral format and the proposed method enables the solution of time dependent systems, including the Navier-Stokes equations with large Reynolds numbers and convective heat transfer problems with large Péclet numbers. Moreover, combining WMIGM with wavelet adaptive analysis holds great appeal as a potentially superior method for solving these intricate problems.

Acknowledgement: The authors sincerely thanks the reviewers and the editors of the journal for the great improvement of this paper.

Funding Statement: This work was supported by the National Natural Science Foundation of China (No. 12172154), the 111 Project (No. B14044), the Natural Science Foundation of Gansu Province (No. 23JRRA1035), and the Natural Science Foundation of Anhui University of Finance and Economics (No. ACKYC20043).

Author Contributions: The authors confirm contribution to the paper as follows: study conception and design: Jiaqun Wang, Xiaojing Liu; coding: Jiaqun Wang, Guanxu Pan; analysis and interpretation of results: Guanxu Pan, Xiaojing Liu; funding support: Jiaqun Wang, Youhe Zhou, Xiaojing Liu; draft manuscript preparation: Jiaqun Wang, Guanxu Pan; draft review: Youhe Zhou, Xiaojing Liu. All authors reviewed the results and approved the final version of the manuscript.

Availability of Data and Materials: The data that support the findings of this study are available from the corresponding author upon reasonable request.

Conflicts of Interest: The authors declare that they have no conflicts of interest to report regarding the present study.

References

1. Kadalbajoo, M. K., Kumar, D. (2008). A non-linear single step explicit scheme for non-linear two-point singularly perturbed boundary value problems via initial value technique. *Applied Mathematics and Computation*, 202(2), 738–746. <https://doi.org/10.1016/j.amc.2008.03.015>
2. Geng, F. Z., Tang, Z. Q. (2016). Piecewise shooting reproducing kernel method for linear singularly perturbed boundary value problems. *Applied Mathematics Letters*, 62, 1–8. <https://doi.org/10.1016/j.aml.2016.06.009>
3. Liu, C. S., Chang, C. W. (2022). Modified asymptotic solutions for second-order nonlinear singularly perturbed boundary value problems. *Mathematics and Computers in Simulation*, 193, 139–152. <https://doi.org/10.1016/j.matcom.2021.10.005>

4. Reddy, N. R., Mohapatra, J. (2015). An efficient numerical method for singularly perturbed two point boundary value problems exhibiting boundary layers. *National Academy Science Letters*, 38(4), 355–359. <https://doi.org/10.1007/s40009-015-0350-z>
5. Kadalbajoo, M. K., Arora, P. (2010). B-splines with artificial viscosity for solving singularly perturbed boundary value problems. *Mathematical and Computer Modelling*, 52(5–6), 654–666. <https://doi.org/10.1016/j.mcm.2010.04.012>
6. Lodhi, R. K., Mishra, H. K. (2017). Quintic B-spline method for solving second order linear and nonlinear singularly perturbed two-point boundary value problems. *Journal of Computational and Applied Mathematics*, 319, 170–187. <https://doi.org/10.1016/j.cam.2017.01.011>
7. Thula, K. (2020). A sixth-order numerical method based on shishkin mesh for singularly perturbed boundary value problems. *Iranian Journal of Science and Technology, Transactions A: Science*, 46, 161–171. <https://doi.org/10.1007/s40995-020-00952-x>
8. Lodhi, R. K., Mishra, H. K. (2018). Septic B-spline method for second order self-adjoint singularly perturbed boundary-value problems. *Ain Shams Engineering Journal*, 9(4), 2153–2161. <https://doi.org/10.1016/j.asej.2016.09.016>
9. Zhu, P., Xie, S. L. (2014). Higher order uniformly convergent continuous/discontinuous Galerkin methods for singularly perturbed problems of convection-diffusion type. *Applied Numerical Mathematics*, 76, 48–59. <https://doi.org/10.1016/j.apnum.2013.10.001>
10. Kaushik, A., Vashishth, A. K., Kumar, V., Sharma, M. (2019). A modified graded mesh and higher order finite element approximation for singular perturbation problems. *Journal of Computational Physics*, 395, 275–285. <https://doi.org/10.1016/j.jcp.2019.04.073>
11. Ma, G. L., Stynes, M. (2020). A direct discontinuous Galerkin finite element method for convection-dominated two-point boundary value problems. *Numerical Algorithms*, 83(2), 741–765. <https://doi.org/10.1007/s11075-019-00701-1>
12. Zhang, J., Ma, X. Q., Lv, Y. H. (2021). Finite element method on Shishkin mesh for a singularly perturbed problem with an interior layer. *Applied Mathematics Letters*, 121, 107509. <https://doi.org/10.1016/j.aml.2021.107509>
13. Reddy, J. N., Martinez, M. (2021). A dual mesh finite domain method for steady-state convection-diffusion problems. *Computers & Fluids*, 214, 104760. <https://doi.org/10.1016/j.compfluid.2020.104760>
14. Lin, B., Li, K., Cheng, Z. (2009). B-spline solution of a singularly perturbed boundary value problem arising in biology. *Chaos, Solitons & Fractals*, 42(5), 2934–2948. <https://doi.org/10.1016/j.chaos.2009.04.036>
15. Vulcanovic, R., Nhan, T. A. (2021). An improved Kellogg-Tsan solution decomposition in numerical methods for singularly perturbed convection-diffusion problems. *Applied Numerical Mathematics*, 170, 128–145. <https://doi.org/10.1016/j.apnum.2021.07.019>
16. Das, P., Natesan, S. (2013). Richardson extrapolation method for singularly perturbed convection-diffusion problems on adaptively generated mesh. *Computer Modeling in Engineering & Sciences*, 90(6), 463–485. <https://doi.org/10.3970/cmescs.2013.090.463>
17. Kadalbajoo, M. K., Gupta, V. (2010). A brief survey on numerical methods for solving singularly perturbed problems. *Applied Mathematics and Computation*, 217(8), 3641–3716. <https://doi.org/10.1016/j.amc.2010.09.059>
18. Kadalbajoo, M. K., Patidar, K. C. (2002). A survey of numerical techniques for solving singularly perturbed ordinary differential equations. *Applied Mathematics and Computation*, 130(2), 457–510. [https://doi.org/10.1016/S0096-3003\(01\)00112-6](https://doi.org/10.1016/S0096-3003(01)00112-6)
19. Linß, T. (2003). Layer-adapted meshes for convection–diffusion problems. *Computer Methods in Applied Mechanics and Engineering*, 192(9–10), 1061–1105. [https://doi.org/10.1016/s0045-7825\(02\)00630-8](https://doi.org/10.1016/s0045-7825(02)00630-8)
20. Stynes, M. (2005). Steady-state convection-diffusion problems. *Acta Numerica*, 14, 445–508. <https://doi.org/10.1017/S0962492904000261>

21. Zhu, P., Xie, S. L. (2020). A uniformly convergent weak galerkin finite element method on shishkin mesh for 1d convection-diffusion problem. *Journal of Scientific Computing*, 85(2), 34. <https://doi.org/10.1007/s10915-020-01345-3>
22. Wang, Y., Meng, X. Y., Li, Y. H. (2021). The finite volume element method on the Shishkin mesh for a singularly perturbed reaction-diffusion problem. *Computers & Mathematics with Applications*, 84, 112–127. <https://doi.org/10.1016/j.camwa.2020.12.011>
23. Lv, Y. H., Zhang, J. (2022). Convergence and supercloseness of a finite element method for a two-parameter singularly perturbed problem on Shishkin triangular mesh. *Applied Mathematics and Computation*, 416, 126753. <https://doi.org/10.1016/j.amc.2021.126753>
24. Zhang, J., Liu, X. W. (2020). Convergence of a finite element method on a Bakhvalov-type mesh for singularly perturbed reaction-diffusion equation. *Applied Mathematics and Computation*, 385, 125403. <https://doi.org/10.1016/j.amc.2020.125403>
25. Zhang, J., Lv, Y. H. (2021). High-order finite element method on a Bakhvalov-type mesh for a singularly perturbed convection-diffusion problem with two parameters. *Applied Mathematics and Computation*, 397, 125953. <https://doi.org/10.1016/j.amc.2021.125953>
26. Zhang, J., Lv, Y. H. (2021). Finite element method for singularly perturbed problems with two parameters on a Bakhvalov-type mesh in 2D. *Numerical Algorithms*, 90, 447–475. <https://doi.org/10.1007/s11075-021-01194-7>
27. Zhang, J., Lv, Y. (2022). Supercloseness of finite element method on a Bakhvalov-type mesh for a singularly perturbed problem with two parameters. *Applied Numerical Mathematics*, 171, 329–352. <https://doi.org/10.1016/j.apnum.2021.09.010>
28. Li, S., Liu, W. K. (1996). Moving least-square reproducing kernel method Part II: Fourier analysis. *Computer Methods in Applied Mechanics and Engineering*, 139(1), 159–193. [https://doi.org/10.1016/S0045-7825\(96\)01082-1](https://doi.org/10.1016/S0045-7825(96)01082-1)
29. Golbabai, A., Kalarestaghi, N. (2018). Improved localized radial basis functions with fitting factor for dominated convection-diffusion differential equations. *Engineering Analysis with Boundary Elements*, 92, 124–135. <https://doi.org/10.1016/j.enganabound.2017.10.008>
30. Wang, J. F., Wu, Y., Xu, Y., Sun, F. X. (2023). A dimension-splitting variational multiscale element-free galerkin method for three-dimensional singularly perturbed convection-diffusion problems. *Computer Modeling in Engineering & Sciences*, 135(1), 341–356. <https://doi.org/10.32604/cmescs.2022.023140>
31. Nguyen, V. P., Rabczuk, T., Bordas, S., Duflo, M. (2008). Meshless methods: A review and computer implementation aspects. *Mathematics and Computers in Simulation*, 79(3), 763–813. <https://doi.org/10.1016/j.matcom.2008.01.003>
32. Liu, G. R. (2009). *Meshfree methods: Moving beyond the finite element method*, 2nd ed. Boca Raton: CRC Press.
33. Tayebi, A., Shekari, Y., Heydari, M. H. (2017). A meshless method for solving two-dimensional variable-order time fractional advection-diffusion equation. *Journal of Computational Physics*, 340, 655–669. <https://doi.org/10.1016/j.jcp.2017.03.061>
34. Barik, N. B., Sekhar, T. V. S. (2017). An efficient local RBF meshless scheme for steady convection-diffusion problems. *International Journal of Computational Methods*, 14(6), 1750064. <https://doi.org/10.1142/s0219876217500645>
35. Shen, Q. (2010). Local RBF-based differential quadrature collocation method for the boundary layer problems. *Engineering Analysis with Boundary Elements*, 34(3), 213–228. <https://doi.org/10.1016/j.enganabound.2009.10.004>
36. Zhang, X. H., Xiang, H. (2014). Variational multiscale element free Galerkin method for convection-diffusion-reaction equation with small diffusion. *Engineering Analysis with Boundary Elements*, 46, 85–92. <https://doi.org/10.1016/j.enganabound.2014.05.010>

37. Zhang, X. H., Zhang, P., Qin, W. J., Shi, X. T. (2021). An adaptive variational multiscale element free Galerkin method for convection-diffusion equations. *Engineering with Computers*, 38, 3373–3390. <https://doi.org/10.1007/s00366-021-01469-6>
38. Li, S., Liu, W. K. (1999). Reproducing kernel hierarchical partition of unity, Part II—applications. *International Journal for Numerical Methods in Engineering*, 45(3), 289–317. [https://doi.org/10.1002/\(SICI\)1097-0207\(19990530\)45:3<289::AID-NME584>3.0.CO;2-P](https://doi.org/10.1002/(SICI)1097-0207(19990530)45:3<289::AID-NME584>3.0.CO;2-P)
39. Li, B., Chen, X. (2014). Wavelet-based numerical analysis: A review and classification. *Finite Elements in Analysis and Design*, 81, 14–31. <https://doi.org/10.1016/j.finel.2013.11.001>
40. Azdoud, Y., Cheng, J., Ghosh, S. (2017). Wavelet-enriched adaptive crystal plasticity finite element model for polycrystalline microstructures. *Computer Methods in Applied Mechanics and Engineering*, 327, 36–57. <https://doi.org/10.1016/j.cma.2017.08.026>
41. Cui, X., Yao, X., Wang, Z., Liu, M. (2017). A hybrid wavelet-based adaptive immersed boundary finite-difference lattice Boltzmann method for two-dimensional fluid–structure interaction. *Journal of Computational Physics*, 333, 24–48. <https://doi.org/10.1016/j.jcp.2016.12.019>
42. Zhou, Y. H. (2021). *Wavelet numerical method and its applications in nonlinear problems*. Singapore: Springer Nature Singapore Pte Ltd.
43. Zuo, H., Yang, Z., Chen, X., Xie, Y., Miao, H. (2015). Analysis of laminated composite plates using wavelet finite element method and higher-order plate theory. *Composite Structures*, 131, 248–258. <https://doi.org/10.1016/j.compstruct.2015.04.064>
44. Vasilyev, O. V., Bowman, C. (2000). Second-generation wavelet collocation method for the solution of partial differential equations. *Journal of Computational Physics*, 165(2), 660–693. <https://doi.org/10.1006/jcph.2000.6638>
45. Fujii, M., Hofer, W. J. R. (2003). Interpolating wavelet collocation method of time dependent Maxwell's equations: Characterization of electrically large optical waveguide discontinuities. *Journal of Computational Physics*, 186(2), 666–689. [https://doi.org/10.1016/S0021-9991\(03\)00091-3](https://doi.org/10.1016/S0021-9991(03)00091-3)
46. Schneider, K., Vasilyev, O. V. (2010). Wavelet methods in computational fluid dynamics. *Annual Review of Fluid Mechanics*, 42(1), 473–503. <https://doi.org/10.1146/annurev-fluid-121108-145637>
47. Brown-Dymkoski, E., Vasilyev, O. V. (2017). Adaptive-anisotropic wavelet collocation method on general curvilinear coordinate systems. *Journal of Computational Physics*, 333, 414–426. <https://doi.org/10.1016/j.jcp.2016.12.040>
48. Zhang, L., Wang, J. Z., Liu, X. J., Zhou, Y. H. (2017). A wavelet integral collocation method for nonlinear boundary value problems in physics. *Computer Physics Communications*, 215, 91–102. <https://doi.org/10.1016/j.cpc.2017.02.017>
49. Yang, S. Y., Ni, G. Z., Ho, S. L., Machado, J. M., Rahman, M. A. et al. (2000). Wavelet-Galerkin method for computations of electromagnetic fields-computation of connection coefficients. *IEEE Transactions on Magnetics*, 36(4), 644–648. <https://doi.org/10.1109/20.877532>
50. Kim, J. E., Jang, G. W., Kim, Y. Y. (2003). Adaptive multiscale wavelet-Galerkin analysis for plane elasticity problems and its applications to multiscale topology design optimization. *International Journal of Solids and Structures*, 40(23), 6473–6496. [https://doi.org/10.1016/S0020-7683\(03\)00417-7](https://doi.org/10.1016/S0020-7683(03)00417-7)
51. Liu, X. J., Zhou, Y. H., Wang, X. M., Wang, J. Z. (2013). A wavelet method for solving a class of nonlinear boundary value problems. *Communications in Nonlinear Science and Numerical Simulation*, 18(8), 1939–1948. <https://doi.org/10.1016/j.cnsns.2012.12.010>
52. Liu, X. J., Wang, J. Z., Zhou, Y. H. (2017). A space–time fully decoupled wavelet Galerkin method for solving a class of nonlinear wave problems. *Nonlinear Dynamics*, 90(1), 599–616. <https://doi.org/10.1007/s11071-017-3684-x>
53. Wang, J. Q., Liu, X. J., Zhou, Y. H. (2018). A high-order accurate wavelet method for solving Schrödinger equations with general nonlinearity. *Applied Mathematics and Mechanics*, 39(2), 275–290. <https://doi.org/10.1007/s10483-018-2299-6>

54. Liu, X. J., Liu, G. R., Wang, J. Z., Zhou, Y. H. (2019). A wavelet multiresolution interpolation Galerkin method for targeted local solution enrichment. *Computational Mechanics*, 64(4), 989–1016. <https://doi.org/10.1007/s00466-019-01691-6>
55. Liu, X. J., Liu, G. R., Wang, J. Z., Zhou, Y. H. (2020). A wavelet multiresolution interpolation Galerkin method with effective treatments for discontinuity for crack growth analyses. *Engineering Fracture Mechanics*, 225, 106836. <https://doi.org/10.1016/j.engfracmech.2019.106836>
56. Donoho, D. L. (1992). Interpolating wavelet transforms. *Technical Report*. Department of Statistics, Stanford University, USA.
57. Tobiska, L. (2006). Analysis of a new stabilized higher order finite element method for advection–diffusion equations. *Computer Methods in Applied Mechanics and Engineering*, 196(1), 538–550. <https://doi.org/10.1016/j.cma.2006.05.009>
58. Linß, T. (2001). The necessity of Shishkin decompositions. *Applied Mathematics Letters*, 14(7), 891–896. [https://doi.org/10.1016/S0893-9659\(01\)00061-1](https://doi.org/10.1016/S0893-9659(01)00061-1)
59. Geng, F. Z., Qian, S. P., Li, S. (2014). Numerical solutions of singularly perturbed convection-diffusion problems. *International Journal of Numerical Methods for Heat & Fluid Flow*, 24(6), 1268–1274. <https://doi.org/10.1108/hff-01-2013-0033>
60. Liu, C. S. (2018). Solving singularly perturbed problems by a weak-form integral equation with exponential trial functions. *Applied Mathematics and Computation*, 329, 154–174. <https://doi.org/10.1016/j.amc.2018.02.002>
61. Mohsen, A., El-Gamel, M. (2008). On the Galerkin and collocation methods for two-point boundary value problems using sinc bases. *Computers & Mathematics with Applications*, 56(4), 930–941. <https://doi.org/10.1016/j.camwa.2008.01.023>
62. Shah, F. A., Abass, R. (2017). An efficient wavelet-based collocation method for handling singularly perturbed boundary-value problems in fluid mechanics. *International Journal of Nonlinear Sciences and Numerical Simulation*, 18(6), 485–494. <https://doi.org/10.1515/ijnsns-2016-0063>
63. Kumar, M., Mishra, H. K., Singh, P. (2009). A boundary value approach for a class of linear singularly perturbed boundary value problems. *Advances in Engineering Software*, 40(4), 298–304. <https://doi.org/10.1016/j.advengsoft.2008.04.012>
64. Xu, M. T. (2017). A type of high order schemes for steady convection-diffusion problems. *International Journal of Heat and Mass Transfer*, 107, 1044–1053. <https://doi.org/10.1016/j.ijheatmasstransfer.2016.10.128>
65. Johnston, H., Mortari, D. (2021). Least-squares solutions of boundary-value problems in hybrid systems. *Journal of Computational and Applied Mathematics*, 393, 113524. <https://doi.org/10.1016/j.cam.2021.113524>
66. Kumar, V., Srinivasan, B. (2015). An adaptive mesh strategy for singularly perturbed convection diffusion problems. *Applied Mathematical Modelling*, 39(7), 2081–2091. <https://doi.org/10.1016/j.apm.2014.10.019>
67. Dubey, R. K., Gupta, V. (2020). A mesh refinement algorithm for singularly perturbed boundary and interior layer problems. *International Journal of Computational Methods*, 17(7), 1950024. <https://doi.org/10.1142/s0219876219500245>